Reaction of Zoledronate with β-Tricalcium Phosphate for the Design of Potential Drug Device Combined Systems

Hélène Roussière,[†,‡,§] Franck Fayon,[△] Bruno Alonso,[△] Thierry Rouillon,[†] Verena Schnitzler,[‡,§] Elise Verron,[†] Jérôme Guicheux,[†] Marc Petit,[‡,§] Dominique Massiot,[△] Pascal Janvier,[‡,§] Jean-Michel Bouler,[†] and Bruno Bujoli*[,‡,§]

Laboratoire d'Ingénierie Ostéo-articulaire et Dentaire (LIOAD), Faculté de Chirurgie Dentaire, Nantes Atlantique Universités, INSERM, UMRS 791, BP 84215, 44042 Nantes Cedex 1, France, Université de Nantes, Laboratoire de Synthèse Organique, Faculté des Sciences et des Techniques, 2 rue de la Houssinière, BP 92208, 44322 Nantes Cedex 3, France, CNRS, UMR 6513, BP 92208, 44322 Nantes Cedex 3, France, and CRMHT, UPR CNRS 4212, 1D Avenue de la Recherche Scientifique, 45071 Orléans Cedex 02, France

Received September 11, 2007. Revised Manuscript Received November 5, 2007

The reaction of aqueous Zoledronate solutions with β-tricalcium phosphate resulted in the precipitation of a crystalline Zoledronate complex on the surface of the calcium phosphate. This complex $(CaNa[(HO)(C_4H_5N_2)C(PO_3)(PO_3H)]\cdot xH_2O)$ was found to be metastable, leading to a pure calcium complex $[Ca_3[(HO)(C_4H_5N_2)C(PO_3)(PO_3H)]_2\cdot xH_2O]$ upon washing with water. This latter compound was found to release the bisphosphonate in phosphate buffers, in direct proportion to the phosphate concentration, while using a specific in vitro bone resorption model, an inhibition of osteoclastic activity was observed with this material. This suggested that when this composite is implanted in bone tissues, the drug will be released in greater concentration the more the bone is being resorbed, resulting in a decrease of osteoclast activity and making this drug device combination suitable for practical application as a bisphosphonate local delivery system. In addition, the chemical environment of the bisphosphonate moiety in the two reported bisphosphonate/calcium phosphate composites was probed using ^{31}P and ^{23}Na magic-angle-spinning NMR and two-dimensional ^{31}P homonuclear and $^{31}P-^{1}H$ heteronuclear correlation experiments, thus giving clear evidence that modern high-resolution solid-state NMR is a powerful tool for the characterization of calcium phosphate-based biomaterials.

Introduction

Porous calcium phosphate ceramics have been used extensively as bioactive implants in human bone surgery because of their similarity to the mineral component of bone.[1–7] Indeed, such biomaterials with suitable composition and porosity are slowly resorbed in the body, to be replaced by natural bone by the same processes active in bone remodeling. Bisphosphonates (BPs) are of widespread use for the treatment of various metabolic bone diseases, including postmenopausal osteoporosis, because of their potent inhibitory effect on osteoclastic bone resorption.[8–14] Taking account of the affinity of BPs for bone, studies from Denissen et al.,[15–19] Tanzer et al.,[20] and Yoshinari et al.[21] were focused on hydroxyapatite (HAp)/BP combinations, and

* Corresponding author. E-mail: bruno.bujoli@univ-nantes.fr. Fax: +33 251125402.
† Nantes Atlantique Universités, INSERM, UMRS 791.
‡ Université de Nantes.
§ CNRS, UMR 6513.
△ CRMHT, UPR CNRS 4212.

(1) Vallet-Regi, M.; Gonzalez-Calbet, J. M. Calcium phosphates as substitution of bone tissues. *Prog. Solid State Chem.* **2004**, *32* (1–2), 1–31.
(2) Ransford, A. O.; Morley, T.; Edgar, M. A.; Webb, P.; Passuti, N.; Chopin, D.; Morin, C.; Michel, F.; Garin, C.; Pries, D. Synthetic porous ceramic compared with autograft in scoliosis surgery. A prospective, randomized study of 341 patients. *J. Bone Jt. Surg., Br. Vol.* **1998**, *80* (1), 13–8.
(3) Passuti, N.; Daculsi, G.; Rogez, J. M.; Martin, S.; Bainvel, J. V. Macroporous calcium phosphate ceramic performance in human spine fusion. *Clin. Orthop.* **1989**, *46* (248), 169–176.
(4) Passuti, N.; Daculsi, G. Calcium phosphate ceramics in orthopedic surgery. *Presse Med.* **1989**, *18* (1), 28–31.
(5) Gouin, F.; Delecrin, J.; Passuti, N.; Touchais, S.; Poirier, P.; Bainvel, J. V. Filling of bone defects using biphasic macroporous calcium phosphate ceramic. Apropos of 23 cases. *Rev. Chir. Orthop. Reparatrice Appar. Mot.* **1995**, *81* (1), 59–65.
(6) Dorozhkin, S.; Epple, M. Biological and medical significance of calcium phosphates. *Angew. Chem., Int. Ed.* **2002**, *41*, 3130–3146.
(7) Cavagna, R.; Daculsi, G.; Bouler, J. Macroporous calcium phosphate ceramic: a prospective study of 106 cases in lumbar spinal fusion. *J. Long-Term Eff. Med. Implants* **1999**, *9* (4), 403–412.
(8) Yaffe, A.; Kollerman, R.; Bahar, H.; Binderman, I. The influence of alendronate on bone formation and resorption in a art ectopic bone development model. *J. Periodontol.* **2003**, *74*, 44–50.
(9) Wilder, L.; Jaeggi, K. A.; Glatt, M.; Müller, K.; Bachmann, R.; Bisping, M.; Born, A.; Cortesi, R.; Guiglia, G.; Jeker, H.; Klein, R.; Ramseier, U.; Schmid, J.; Schreiber, G.; Seltenmeyer, Y.; Green, J. R. Highly potent geminal bisphosphonates. From pamidronate (Aredia) to zoledronic acid (Zometa). *J. Med. Chem.* **2002**, *45*, 3721–3738.
(10) Rodan, G. A.; Martin, T. J. Therapeutic approaches to bone diseases. *Science* **2000**, *289*, 1508–1514.
(11) Fleisch, H. The role of bisphosphonates in breast cancer: Development of bisphosphonates. *Breast Cancer Res.* **2002**, *4*, 30–34.
(12) Fleisch, H. The bisphosphonate ibandronate, given daily as well as discontinuously, decreases bone resorption and increases calcium retention as assessed by 45 Ca kinetics in the intact rat. *Osteoporosis Int.* **1996**, *6*, 166–170.
(13) Fisher, J. E.; Rodan, G. A.; Reszka, A. A. In vivo effects of bisphosphonates on the osteoclast mevalonate pathway. *Endocrinology* **2000**, *141*, 4793–4796.
(14) Arden-Cordone, M.; Siris, E.; Lyles, K.; Knieriem, A.; Newton, R.; Schaffer, V.; Zelenakas, K. Antiresorptive effect of a single infusion of microgram quantities of zoledronate in Paget's disease of bone. *Calcif. Tissue Int.* **1997**, *60*, 415–418.

10.1021/cm702584d CCC: $40.75
Published on Web 12/05/2007

the local elution of the BP from the implant was found to promote substantial bone augmentation around the implantation site. In all cases, however, no investigation of the nature of the BP/HAp interaction was performed, and the amount of drug loaded on the implant was not determined. Similarly, bone augmentation around HAp-coated metal implants was recently reported by us, when chemically modified using BPs (Zoledronate) and then implanted either in healthy[22] or osteoporotic[23] bone sites. This approach, in which a local delivery of the drug is provided, could offer a convenient strategy to avoid adverse effects commonly observed for systemic BP treatments (like fever,[24,25] ulcers,[26] or osteonecrosis of the jaw[27,28]) and increase the BP bioavailability that is usually low for oral administration.[29,30] In addition, Nancollas et al.[31] measured the binding affinities for HAp of six BPs (Zoledronate > Alendronate > Ibandronate > Risedronate > Etidronate > Clodronate), which were found to be consistent with observed clinical differences among these BPs.[32] Finally, the interaction of five BPs with the (001), (010), and (100) crystallographic faces of HAp was modeled by Robinson et al.,[33] using the generalized AMBER force field.

Scheme 1. Schematic Representation of the Chemical Association of BPs onto the Surface of CDA Particles, via a Reversible BP for Phosphate Exchange

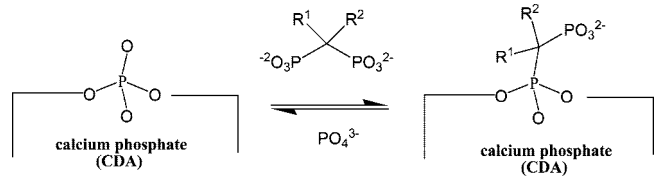

Moreover, we have recently shown that calcium-deficient apatites (CDAs) were also appropriate carriers for *gem*-BP antiresorptive drugs, in which the CDA/BP association can be chemically controlled and characterized.[34–36] Indeed, we have reported that the reaction of CDA powders with aqueous *gem*-BP solutions resulted in a surface adsorption of the drug, driven by PO_3 for PO_4 exchange (Scheme 1). In this context, we have then shown that the main parameter governing the release of the BP sorbed onto CDAs was the phosphate concentration in the desorption medium, with release kinetics compatible with the inhibition of bone resorption.[34] This suggests that BP-loaded CDAs might be used as implants for the local elution of the drug at the main osteoporosis-induced fracture sites (femur neck, distal radius, and vertebral bodies) and result in bone consolidation.

There is still a great deal left to understand and learn about the potential of calcium phosphate/BP combinations as implants for local drug delivery. Here, we report on a novel type of chemical behavior observed in the case of β-tricalcium phosphate [β-TCP, β-$Ca_3(PO_4)_2$], when reacted with Zoledronate in an aqueous medium, for which the formation of crystalline needles of a Zoledronate complex on the β-TCP surface takes place (Scheme 2). Such composites will differ from BP-loaded CDAs on two points: (i) the resorbability is lower for β-TCP compared to that of CDA; (ii) the BP/calcium phosphate chemical association is radically different, and accordingly the BP release should be different. Another

(15) Denissen, H.; Martinetti, R.; van Lingen, A.; van den Hooff, A. Normal osteoconduction and repair in and around submerged highly bisphosphonate-complexed hydroxyapatite implants in rat tibiae. *J. Periodontol.* **2000**, *71* (2), 272–278.
(16) Denissen, H.; Montanari, C.; Martinetti, R.; van Lingen, A.; van den Hooff, A. Alveolar bone response to submerged bisphosphonate-complexed hydroxyapatite implants. *J. Periodontol.* **2000**, *71* (2), 279–286.
(17) Denissen, H.; van Beek, E.; Lowik, C.; Papapoulos, S.; van den Hooff, A. Ceramic Hydroxyapatite Implants for the Release of Bisphosphonate. *Bone Miner.* **1994**, *25* (2), 123–134.
(18) Denissen, H.; van Beek, E.; Martinetti, R.; Klein, C.; van der Zee, E.; Ravaglioli, A. Net-shaped hydroxyapatite implants for release of agents modulating periodontal-like tissues. *J. Periodontal Res.* **1997**, *32* (1), 40–46.
(19) Denissen, H.; van Beek, E.; van den Bos, T.; DeBlieck, J.; Klein, C.; van den Hooff, A. Degradable bisphosphonate−alkaline phosphatase-complexed hydroxyapatite implants in vitro. *J. Bone Miner. Res.* **1997**, *12* (2), 290–297.
(20) Tanzer, M.; Karabasz, D.; Krygier, J. J.; Cohen, R.; Bobyn, J. D. The Otto Aufranc award. Bone augmentation around and within porous implants by local bisphosphonate elution. *Clin. Orthop. Relat. Res.* **2005**, *441*, 30–39.
(21) Yoshinari, M.; Oda, Y.; Inoue, T.; Matsuzaka, K.; Shimono, M. Bone response to calcium phosphate-coated and bisphosphonate-immobilized titanium implants. *Biomaterials* **2002**, *23*, 2879–2885.
(22) Peter, B.; Pioletti, D. P.; Laib, S.; Bujoli, B.; Pilet, P.; Janvier, P.; Guicheux, J.; Zambelli, P.-Y.; Bouler, J.-M.; Gauthier, O. Calcium phosphate drug delivery system: influence of local zoledronate release on bone implant osteointegration. *Bone* **2005**, *36* (1), 52–60.
(23) Peter, B.; Gauthier, O.; Laïb, S.; Bujoli, B.; Guicheux, J.; Janvier, P.; Harry Van Lenthe, G.; Muller, R.; Zambelli, P.-Y.; Bouler, J.-M.; Pioletti, D. P. Local delivery of bisphosphonate from coated orthopedic implants increases implants mechanical stability in osteoporotic rats. *J. Biomed. Mater. Res.* **2006**, *76A* (1), 133–143.
(24) Thiebaud, D.; Sauty, A.; Burckhardt, P.; Leuenberger, P.; Sitzler, L.; Green, J. R.; Kandra, A.; Zieschang, J.; Ibarra de Palacios, P. An in vitro and in vivo study of cytokines in the acute-phase response associated with bisphosphonates. *Calcif. Tissue Int.* **1997**, *61* (5), 386–392.
(25) Gallacher, S. J.; Ralston, S. H.; Patel, U.; Boyle, I. T. Side-effects of pamidronate. *Lancet* **1989**, *2*, 42–43.
(26) Elliott, S. N.; McKnight, W.; Davies, N. M.; MacNaughton, W. K.; Wallace, J. L. Alendronate induces gastric injury and delays ulcer healing in rodents. *Life Sci.* **1997**, *62* (1), 77–91.
(27) Purcell, P. M.; Boyd, I. W. Bisphosphonates and osteonecrosis of the jaw. *Med. J. Aust.* **2005**, *182* (8), 417–418.
(28) Migliorati, C. A. Bisphosphonates an oral cavity avascular bone necrosis. *J. Clin. Oncol.* **2003**, *21* (22), 4253–4254.
(29) Vachal, P.; Hale, J. J.; Lu, Z.; Streckfuss, E. C.; Mills, S. G.; MacCoss, M.; Yin, D. H.; Algayer, K.; Manser, K.; Kesisoglou, F.; Ghosh, S.; Alani, L. L. Synthesis and study of alendronate derivatives as potential prodrugs of alendronate sodium for the treatment of low bone density and osteoporosis. *J. Med. Chem.* **2006**.
(30) Hyldstrup, L.; Flesch, G.; Hauffe, S. A. Pharmacokinetic evaluation of pamidronate after oral administration: a study on dose proportionality, absolute bioavailability, and effect of repeated administration. *Calcif. Tissue Int.* **1993**, *53*, 297–300.
(31) Nancollas, G. H.; Tang, R.; Phipps, R. J.; Henneman, Z.; Gulde, S.; Wu, W.; Mangood, A.; Russell, R. G. G.; Ebetino, F. H. Novel insights into actions of bisphosphonates on bone: Differences in interactions with hydroxyapatite. *Bone* **2006**, *38* (5), 617.
(32) Russell, R. G. G. Determinants of structure-function relationships among bisphosphonates. *Bone* **2007**, *40* (5), S21.
(33) Robinson, J.; Cukrowski, I.; Marques, H. M. Modelling the interaction of several bisphosphonates with hydroxyapatite using the generalised AMBER force field. *J. Mol. Struct.* **2006**, *825* (1–3), 134.
(34) Roussiere, H.; Montavon, G.; Laib, S.; Janvier, P.; Alonso, B.; Fayon, F.; Petit, M.; Massiot, D.; Bouler, J.-M.; Bujoli, B. Hybrid materials applied to biotechnologies: coating of calcium phosphates for the design of implants active against bone resorption disorders. *J. Mater. Chem.* **2005**, *15*, 3869–3875.
(35) Josse, S.; Faucheux, C.; Soueidan, A.; Grimandi, G.; Massiot, D.; Alonso, B.; Janvier, P.; Laib, S.; Pilet, P.; Gauthier, O.; Daculsi, G.; Guicheux, J.; Bujoli, B.; Bouler, J.-M. Novel biomaterials for bisphosphonate delivery. *Biomaterials* **2005**, *26* (14), 2073–2080.
(36) Josse, S.; Faucheux, C.; Soueidan, A.; Grimandi, G.; Massiot, D.; Alonso, B.; Janvier, P.; Laïb, S.; Gauthier, O.; Daculsi, G.; Guicheux, J.; Bujoli, B.; Bouler, J.-M. Chemically modified calcium phosphates as novel materials for bisphosphonate delivery. *Adv. Mater.* **2004**, *16*, 1423–1427.

Scheme 2. Schematic Representation of the Reaction of Zoledronate with β-TCP Particles, Leading to the Formation of Crystalline BP Complexes A and B, via a Dissolution/ Precipitation Process

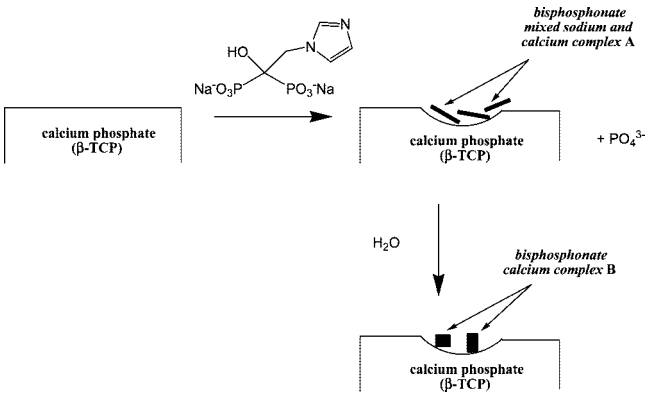

interest of the herein reported composite lies in the fact that most of the calcium phosphate-based biomaterials used clinically are ceramics, all containing significant amounts of β-TCP.

In vivo preclinical studies will be necessary to assess whether β-TCP as a carrier is better for bone healing than CDA, but a prerequisite to these animal studies is a full characterization of the biomaterial to be implanted, which is the purpose of this study, which describes the characterization and chemical and physical properties of the Zoledronate species present in Zoledronate-loaded β-TCPs.

Experimental Section

Synthesis. β-TCP was obtained by hydrolysis of dicalcium phosphate dihydrate powder (40 g; Merck, Darmstadt, Germany) in 500 mL of a 0.3 mol L^{-1} NH_4OH solution. The reaction was performed under gentle stirring during 4 h at 90 °C, and the resulting solid was filtered, rinsed with water, dried in air, and calcined at 1000 °C for 4 h. **TCP+A** was prepared by suspending TCP (40−80 μm; 500 mg) in 2.5 mL of an ultrapure water (18 MΩ cm) solution of zoledronic acid (the disodium form; 70 mg, $C_{\text{Zoledronate}} = 0.07$ mol L^{-1}), in an assay tube that was rotated slowly and mechanically (16 rpm) for 48 h. After centrifugation, the solid was filtered, washed four times with 5 mL of ultrapure water, and allowed to dry at room temperature. The amount of Zoledronate incorporated onto the calcium phosphate phases was determined by difference, after measurement of its residual concentration in the supernatant by total organic carbon (TOC) measurements (Shimadzu TOC 5000A analyzer; the limit of detection of the method was 0.5 ppm of carbon, corresponding to a 8×10^{-6} mol L^{-1} concentration of Zoledronate). The experiment was repeated eight times, leading to a 87.9(1)% Zoledronate incorporation ratio (0.31 mmol g^{-1}) from the solution. **TCP+B**. A total of 500 mg of **TCP+A** was suspended in water (10 mL) for 1 h. The mixture was filtered, and the isolated solid was equilibrated an additional four times in water (10 mL) for 1 h. After final filtration of the solid, which was then dried in air, the filtrates were combined and the amount of Zoledronate released [43.3(6)% of the Zoledronate initially present on the solid] was determined by TOC measurements, which corresponded to a final of 0.17 mmol g^{-1} of Zoledronate still present on the solid.

Desorption Study. TCP+B samples (20 mg) were equilibrated for 48 h in $10^{-1}-10^{-3}$ mol L^{-1} phosphate buffers to study the desorption of the BP as a function of the phosphate concentration, using TOC measurements.

Cellular Effects of Zoledronate Released by TCP+B **Materials.** To investigate the biological activity of **TCP+B**, a well-established osteoclastic model was used, namely, the unfractioned rabbit bone cell model.[37,38] **TCP+B** was mixed with Zoledronate-free β-TCP (1:1000). The powdered sample was compacted at 130 MPa for 30 s (Specac, Kent, U.K.) to obtain 200 mg pellets 10 mm in diameter, which were steam-sterilized at 121 °C for 20 min. Total rabbit bone cells (in 2.5 mL of α-MEM supplemented with 1% penicillin/streptomycin and 1% L-glutamine) were then seeded on dentin slices in six-multiwell plates (5×10^6 cells per dentin slice) in the presence of the diluted **TCP+B** pellets. As an internal control, Zoledronate (10^{-6} mol L^{-1}) or the culture medium alone were also tested on dentin slices. After 4 days, the dentin slices were washed off with sodium hypochlorite and scraped gently using a soft toothbrush to eliminate the cells. The slices were then air-dried, coated with gold palladium, and analyzed by scanning electron microscopy (SEM). The resorption activity of cells was quantified using an image analyzer (LeicaQWin, Wetzlar, Germany) on the whole surface of the dentin slices, and results were expressed as the total resorbed area.

All series of experiments were performed in hexaplicate. Results are expressed as the average of three SEM determinations. Comparative studies of averages were performed using one-way analysis of variance followed by a post hoc test (Fisher's projected least significant difference) with a statistical significance at $p < 0.05$.

Materials and Methods. Zoledronate was a gift from Novartis Pharma Research and was provided as its disodium salt. Transmission electron microscopy (TEM) studies were performed using a JEOL JEM1010 microscope, operating at accelerated voltages of 80 and 100 kV. Selected area electron diffraction (SAED) studies were performed at 80 or 100 kV, with a double tilt holder, and the diffraction constants were calibrated using an evaporated aluminum film as a standard. Energy-dispersive X-ray spectroscopy (EDXS) measurements were performed at 100 kV, using an Oxford Instruments Link ISIS spectrometer, equipped with an ATW2 ultrathin window (energy resolution: 142 eV at 5.9 keV). High-resolution images were obtained on a Hitachi HF2000 field emission gun TEM microscope, operating at 200 kV (resolution: 0.23 nm).

For the TEM and EDXS studies, powdered samples were dispersed either in pure grade ethanol or in filtrated deionized water, and a few drops of the resulting suspensions were deposited on nickel grids covered with a holey carbon film. For each sample, about fifteen EDXS microanalyses were performed, and the mean values and corresponding estimated standard deviations were determined for the measured atomic concentration ratios. Quantitative analyses were obtained on the basis of the Cliff and Lorimer thin film approximation,[39] and the experimental K factors were standardized for calcium, phosphorus, and sodium from analyses performed in the same conditions on sodium pyrophosphate ($Na_4P_2O_7$), β-TCP (β-$Ca_3(PO_4)_2$), and octacalcium phosphate ($Ca_8H_2(PO_4)_6 \cdot 5H_2O$) standards.

In order to determine the C/N ratio present in the different powdered samples, electron probe microanalysis (EPMA or Castaing microprobe) was performed using a CAMECA SX50 micro-

(37) Grimandi, G.; Soueidan, A.; Anjrini, A. A.; Badran, Z.; Pilet, P.; Daculsi, G.; Faucheux, C.; Bouler, J. M.; Guicheux, J. Quantitative and reliable in vitro method combining scanning electron microscopy and image analysis for the screening of osteotropic modulators. *Microsc. Res. Tech.* **2006**, *69* (8), 606–612.

(38) Guicheux, J.; Heymann, D.; Rousselle, A. V.; Gouin, F.; Pilet, P.; Yamada, S.; Daculsi, G. Growth hormone stimulatory effects on osteoclastic resorption are partly mediated by insulin-like growth factor I: An in vitro study. *Bone* **1998**, *22* (1), 25–31.

(39) Cliff, G.; Lorimer, G. W. Quantitative-Analysis of Thin Specimens. *J. Microsc. (Oxford, U.K.)* **1975**, *103* (Mar), 203–207.

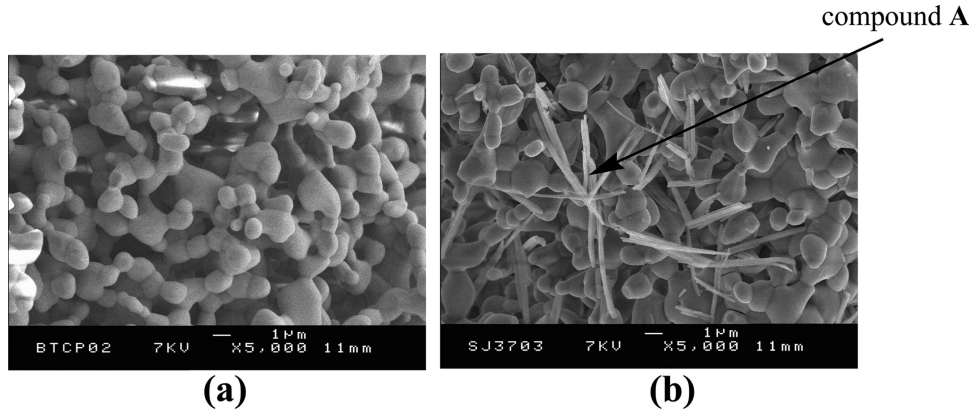

Figure 1. SEM images of pure TCP (a) and **TCP**+**A** (b) (magnitude: 5000).

probe with a Wavelength Dispersive System (WDS) equipped with different dispersive crystals (PC2, PET, TAP, and LiF). Analyses were performed in a scanning mode with a magnification leading to a 200 × 200 μm irradiated area, with a 20 nA beam current and a 10 kV accelerated voltage. A thin layer of aluminum was deposited on the samples by evaporation under vacuum before EPMA analyses. Quantitative analyses were performed after corrections of ZAF effects, using a set of certified MAC standards for X-ray microanalysis (C, BN, $CaSiO_3$, GaP, and $NaAlSi_2O_6$). For each sample, at least six measurements were carried out, and the mean values and estimated standard deviations were determined for the measured C/N ratios. Zoledronate was also studied for comparison.

Powder X-ray diffraction (XRD) patterns of BPs and β-$Ca_{10.5-x/2}$-$Na_x(PO_4)_7$ powders were recorded using a Philips PW 1830 generator equipped with a vertical PW 1050 ($\theta/2\theta$) goniometer and a PW 1711 Xe detector. The data were acquired using Ni-filtered Cu Kα radiation in a step-by-step mode with 2θ initial = 10°, 2θ final = 100°, step 2θ = 0.03°, time per step = 2.3 s. Combined thermogravimetric analysis/differential scanning calorimetry (TGA/DSC) analyses were carried out with a Setaram TG-DSC 11 instrument at a heating rate of 5 °C min^{-1} under compressed air.

The solid-state magic-angle-spinning (MAS) NMR experiments were carried out on Bruker Advance 300 and 750 spectrometers, operating at 7.0 T (^{1}H and ^{31}P Larmor frequencies of 300 and 121.5 MHz) and 17.6 T (^{1}H and ^{31}P Larmor frequencies of 750 and 303.7 MHz), using 4 mm double- and triple-resonance MAS probes.

The ^{31}P{^{1}H} cross-polarization (CP) MAS experiments were performed using a ramped cross-polarization[40] with a contact time of 1 ms. ^{1}H NMR decoupling was achieved using the SPINAL64 sequence[41] with a ^{1}H NMR nutation frequency of 70 kHz. The recycle delay was set to 2 s.

The ^{31}P two-dimensional (2D) through-space double quantum−single quantum MAS correlation spectra of Zoledronate, **TCP**+**A**, and **TCP**+**B** samples were recorded at 7.0 T with a spinning frequency of 10 kHz and a recycle delay of 1 s. For the excitation and reconversion of double-quantum coherences, the C14 recoupling sequence[42] was used with a ^{31}P NMR nutation frequency of 35 kHz. ^{1}H continuous-wave decoupling with a nutation frequency of 75 kHz was applied during the C14 sequences.

The 2D ^{31}P NMR homonuclear proton-driven spin diffusion spectra[43,44] were recorded at 7.0 T with a spinning frequency of 10 kHz. The mixing time was set to 400 ms and the recycle delay to 1 s.

The 2D ^{1}H−^{31}P NMR heteronuclear correlation (HETCOR) experiments[45] on **TCP**+**A** and **TCP**+**B** samples were performed at 17.6 T using Lee−Goldburg cross-polarization[46,47] with a contact time of 750 μs. The frequency-switched Lee−Goldburg (FSLG) ^{1}H NMR homonuclear decoupling sequence[48] (nutation frequency of 50 kHz) was used during the incremented t_1 time evolution to obtain a high-resolution ^{1}H NMR spectrum in the ω_1 dimension.

For all 2D ^{31}P NMR homonuclear and ^{31}P−^{1}H heteronuclear correlation experiments, ^{1}H SPINAL-64 decoupling[41] with a ^{1}H NMR nutation frequency of 70 kHz was applied during both the incremented t_1 evolution period and signal acquisition, and pure absorption phase spectra were obtained using the States method.[49]

The single-pulse ^{23}Na MAS NMR spectra were recorded at 17.6 and 9.4 T, corresponding to ^{23}Na Larmor frequencies of 198.4 and 105.8 MHz, using a $\pi/6$ pulse with a recycle delay of 5 s and a spinning frequency of 12 kHz.

^{1}H, ^{31}P, and ^{23}Na NMR chemical shifts were referenced relative to $Si(CH_3)_4$, a 85% H_3PO_4 solution, and a 1 mol L^{-1} aqueous NaCl solution, respectively.

Results and Discussion

Characterization of the Zoledronate/β-TCP Reaction Product. The reaction of β-TCP with an aqueous solution of Zoledronate led to the formation of a new compound, most likely a BP complex termed **A**, deposited as crystalline needles on the β-TCP surface (Figure 1). Treating β-TCP with increasing quantities of BP ($C_{Zoledronate}$ = 0.01−0.08 mol L^{-1}) resulted in an increase in the amount of crystals formed, along with a nearly constant uptake of the BP (ca. 90%). A sample, denoted as **TCP**+**A**, was selected for the rest of the study, which corresponded to a 0.31 mmol g^{-1} amount of **A** incorporated onto the β-TCP phase, determined using TOC measurements (see the Experimental Section).

(40) Metz, G. X.; Wu, L.; Smith, S. O. *J. Magn. Reson., Ser. A* **1994**, *110*, 219–227.
(41) Fung, B. M.; Khitrin, A. K.; Ermolaev, K. *J. Magn. Reson., Ser. A* **2000**, *142*, 97–101.
(42) Brinkmann, A.; Eden, M.; Levitt, M. *J. Chem. Phys.* **2000**, *112*, 8539–8554.
(43) Schmidt-Rohr, K.; Spiess, H. W. *Multidimensional Solid-State NMR and Polymers*; Academic Press: London, 1994.
(44) Suter, D.; Ernst, R. R. *Phys. Rev. B* **1985**, *32*, 5608–5627.
(45) Caravatti, P.; Braunschweiler, L.; Ernst, R. *Chem. Phys. Lett.* **1983**, *100*, 305–310.
(46) Ladizhansky, V.; Vega, S. *J. Chem. Phys.* **2000**, *112*, 7158–7168.
(47) van Rossum, B. J.; de Groot, C. P.; Ladizhansky, V.; Vega, S.; de Groot, H. J. M. *J. Am. Chem. Soc.* **2000**, *122*, 3465–3472.
(48) Bielecki, A.; Kolbert, A.; Levitt, M. *Chem. Phys. Lett.* **1989**, *155*, 341–346.
(49) States, D. J.; Haberkorn, R. A.; Ruben, D. J. *J. Magn. Reson., Ser. A* **1982**, *48*, 286–292.

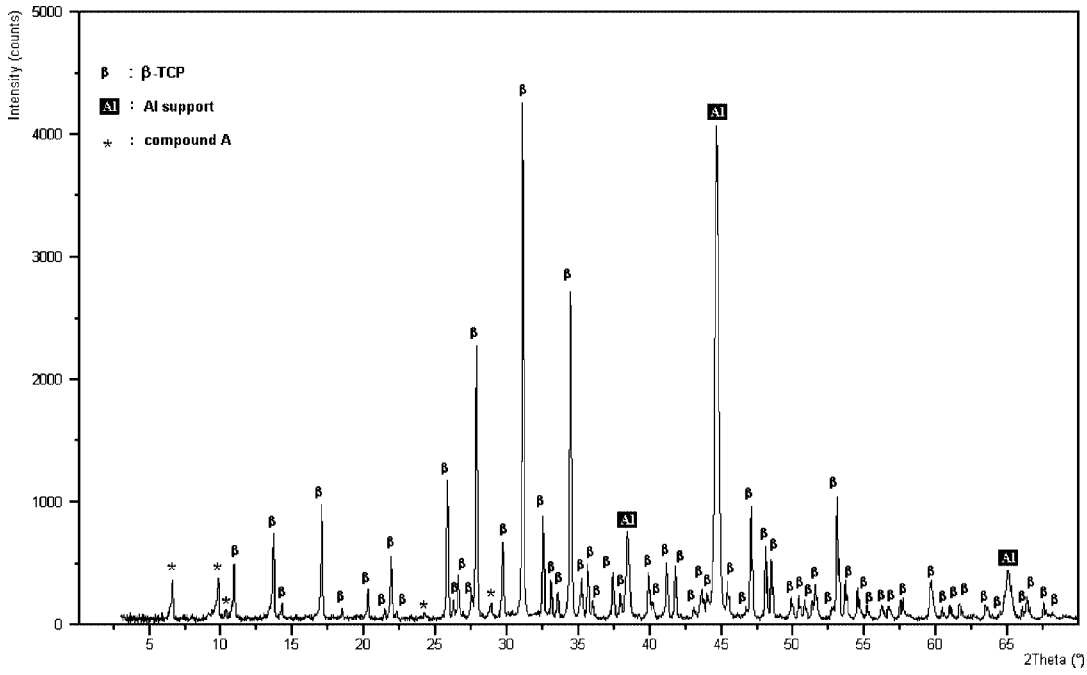

Figure 2. Powder XRD pattern of **TCP**+**A**. Asterisks correspond to diffraction peaks related to compound **A**.

The indexation of the powder XRD pattern recorded for **TCP**+**A** (Figure 2) showed the presence of crystalline β-TCP as the major product, while mainly two additional weak diffraction peaks were observed at high θ values (13.4 and 9.0 Å, respectively), most likely corresponding to compound **A**. Because β-TCP is a ceramic obtained at high temperature (1000 °C), the TGA trace of **TCP**+**A** (Supporting Information) can reasonably be associated with the degradation of complex **A**. The two first endothermic steps (71 and 145 °C) most likely correspond to the release of weakly and strongly bonded water molecules, respectively (observed weight losses: 1.7 and 1.2%, respectively). Then, a complicated stepwise process of hydrogen phosphonate group condensation and burning of organic moieties occurs between 200 and 650 °C (three DSC exothermic peaks observed at 330, 427, and 532 °C, respectively). The transformation is completed at 650 °C, resulting in a white solid after a total weight loss of 8.0%. Identification of the decomposition product of complex **A** was not possible from the powder XRD pattern of the residue, which was dominated by the β-TCP diffraction peaks.

The single-pulse ^{31}P NMR spectrum (not shown) confirmed that the major compound present was β-TCP, while a weak signal was observed in the expected range for BPs (10–20 ppm). ^{31}P{^{1}H} CP MAS NMR experiments were then performed, which allowed one to selectively observe the ^{31}P NMR resonances of the BP moieties while removing the intense signal of the proton-free β-TCP bulk from the ^{31}P NMR spectra. Thus, the solid-state ^{31}P CP MAS NMR spectrum of the **TCP**+**A** sample (Figure 3b) showed a massif containing eight partially overlapping ^{31}P NMR resonances that did not correspond to the starting crystalline Zoledronate (Figure 3a). The narrow line width of these ^{31}P NMR resonances was consistent with the presence of a Zoledronate complex in a crystalline form, in agreement with SEM observations. In order to determine the number of crystalline

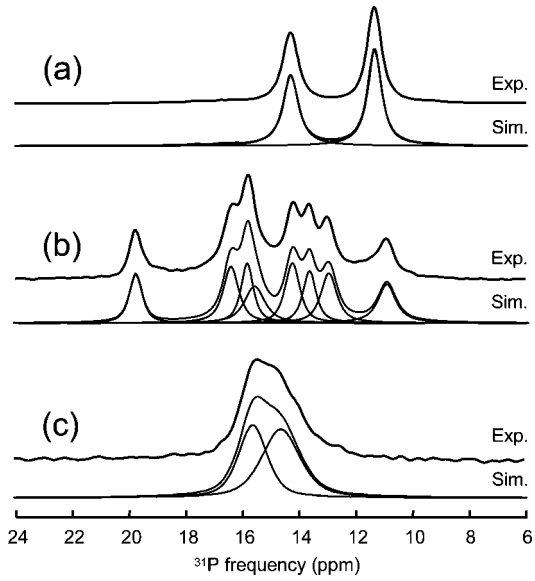

Figure 3. Experimental ^{31}P VACP MAS NMR spectra of Zoledronate (a), **TCP**+**A** (b), and **TCP**+**B** (c) and their simulations according to the parameter given in Table 1. The spectra were recorded at a spinning frequency of 12 kHz and magnetic fields of 7.0 T (a) and 17.6 T (b).

forms of the Zoledronate complex in the **TCP**+**A** sample and their respective number of nonequivalent phosphorus sites, 2D ^{31}P NMR proton-driven magnetization exchange experiments were performed, which allowed one to probe the long-range phosphorus−phosphorus spatial proximities.[43,44] As shown in Figure 4a, the 2D ^{31}P NMR homonuclear correlation spectrum recorded with a mixing time of 400 ms gave evidence of cross-correlation peaks of various intensities between all of the individual ^{31}P NMR resonances displayed in the 1D CP MAS NMR spectrum. This clearly indicates that the BP complex **A** is unambiguously present as a single phase containing eight distinct phosphorus sites. The absence of correlation peaks with the ^{31}P NMR resonances of β-TCP (even at longer mixing time of 1 s) also suggests that the

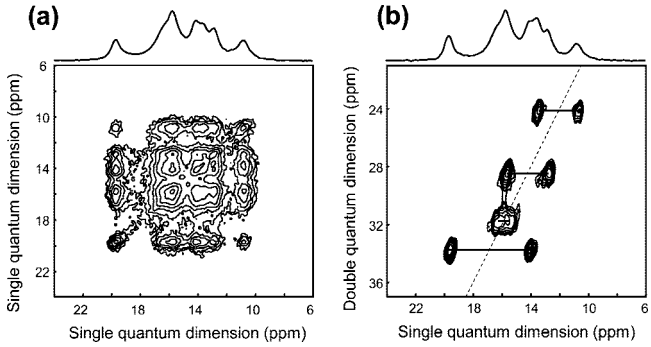

Figure 4. 2D proton-driven magnetization exchange ^{31}P MAS NMR spectrum (a) and 2D homonuclear through-space DQ−SQ correlation ^{31}P MAS NMR spectrum (b) of **TCP+A**, recorded at a magnetic field of 7.0 T and a spinning frequency of 10 kHz.

Table 1. ^{31}P NMR Isotropic Chemical Shift (δ_{ISO}), Full Width at Half-Maximum (fwhm), and Relative Intensities of the Different ^{31}P NMR Resonances in the Starting Zoledronate, TCP+A and TCP+B, Obtained from the Simulation of the 1D CP MAS and 2D DQ−SQ Correlation Spectra

		δ_{ISO} (ppm)	fwhm (ppm)	I (%)
Zoledronate	P(1)	14.3	0.66	47
	P(2)	11.4	0.66	53
TCP+A	P(1)	19.7	0.55	10.1
	P(2)	14.2	0.62	14.3
	P(3)	16.4	0.65	14.5
	P(4)	15.5	0.85	12.2
	P(5)	15.8	0.52	12.3
	P(6)	12.9	0.67	13.2
	P(7)	13.6	0.55	11.4
	P(8)	10.9	0.76	12.0
TCP+B	P(1)	15.6	1.3	44
	P(2)	14.6	1.7	56

BP complex is separated from the calcium phosphate support. In order to determine the number of nonequivalent Zoledronate molecules in **A**, additional ^{31}P NMR homonuclear through-space double quantum−single quantum (DQ−SQ) correlations MAS spectra were recorded. We have used short excitation and reconversion periods of 0.8 ms. This allows both to efficiently probe dipolar couplings of ∼700 Hz characteristic of a P−C−P bond with a P−P distance of ∼0.3 nm and to minimize the contributions of weaker longer-range dipolar couplings (<300 Hz) corresponding to P−P distances larger than 0.4 nm, as was previously demonstrated for recoupling sequences having a similar scaling factor.[50,51] On the 2D DQ−SQ spectrum of **TCP+A**(Figure 4b), four different pairs of cross-correlation peaks were clearly present, corresponding to eight distinct ^{31}P NMR resonances, in contrast to the case of the starting Zoledronate (spectrum not shown), where a single pair of cross-correlation peaks between two distinct P NMR resonances was observed. This demonstrates that the crystalline structure of **A** contains eight distinct phosphorus sites arising from four crystallographically nonequivalent Zoledronate molecules per unit cell, for which a 1:1:1:1 approximate relative intensity ratio was measured from the ^{31}P NMR CP spectrum. The parameters of the eight distinct ^{31}P NMR resonances obtained from the simulation of both 1D CP MAS and 2D homonuclear DQ−SQ correlation spectra are reported in Table 1.

After sonication of a suspension of **TCP+A** in ethanol, different sedimentation times were observed for **A** and β-TCP, showing a more rapid decantation of the latter phase. It was thus possible to isolate a small amount of a sample enriched with **A**, which was studied using TEM, coupled with EDXS. From EDXS analysis measurements of the P/Ca/Na ratio [2:1.08(7):0.93(15) (esd: estimated standard deviation in parentheses)], compound **A** was found to be a mixed sodium and calcium complex, corresponding to the probable following composition: $CaNa[(HO)(C_4H_5N_2)C(PO_3)(PO_3H)]\cdot xH_2O$. We have also checked that the C/N ratio [2.7(2)] was close to the expected value (2.5), using Castaing EPMA, and that its WDS spectrum was close to that recorded for Zoledronate (see the Supporting Information). Very few mixed calcium and sodium BP complexes have been reported in the literature[52] and none with a P/Ca/Na ratio similar to that found in the present study.

In addition, from TEM images and SAED observations, compound **A** appeared as needles of low crystallinity, with a "plate-ribbon"-like morphology and a low thickness (Figure 5a). The needles exhibited a few diffraction reflections along one direction only, with a periodicity ranging from 16 to 22 Å (Figure 5b). Observations were performed with a low intensity of the electron beam, to avoid any damage of the needles. Rotation around the axis corresponding to the periodic order and perpendicular to this axis did not show any additional reflection. Moreover, the periodic axis observed on the SAED pattern did not disappear when rotation was applied perpendicularly to this order axis. This could be due to elongated nodes of the corresponding reciprocal lattice, resulting from factors related to the very thin plate-ribbon-like morphology of compound **A**. High-resolution TEM observations only showed an ordering along one direction, perpendicular to the long axis of the needles, with a periodicity close to 22 Å (Figure 5c), consistent with the observations made from the electron diffraction pattern.

It is worth noting that all attempts to prepare compound **A** directly from Zoledronate and various soluble calcium sources failed. However, when Zoledronate (30 mg) was added to a liquid phase (0.75 mL) resulting from the filtration of a β-TCP suspension (200 mg) in water (1 mL) stirred for 2 days, a small quantity of crystals formed in the solution (less than 1 mg), the P/Ca/Na ratio of which [2:0.93(5):0.68(11)], determined from EDXS measurements, was close to that measured for **A** as well as its morphology and SAED pattern. This observation is consistent with a dissolution/precipitation process involved in the formation of **A**.

The presence of sodium in compound **A** was confirmed by recording ^{23}Na MAS NMR spectra of **TCP+A**. As shown in Figure 6a, the magnetic field dependence of the ^{23}Na MAS NMR spectra suggests the presence of several overlapping

(50) Fayon, F.; Bessada, C.; Coutures, J. P.; Massiot, D. High-resolution double-quantum ^{31}P MAS NMR study of the intermediate-range order in crystalline and glass lead phosphates. *Inorg. Chem.* **1999**, *38* (23), 5212–5218.

(51) Gunne, J.; Eckert, H. High-resolution double-quantum P-31 NMR: A new approach to structural studies of thiophosphates. *Chem.—Eur. J.* **1998**, *4* (9), 1762–1767.

(52) Konturri, M.; Peräniemi, S.; Vepsäläinen, J. J.; Ahlgrèn, M. A structural study of bisphosphonate mrtal complexes—Three new polymeric structures of the calcium complex of clodronic acid. *Eur. J. Inorg. Chem.* **2004**, 2627–2631.

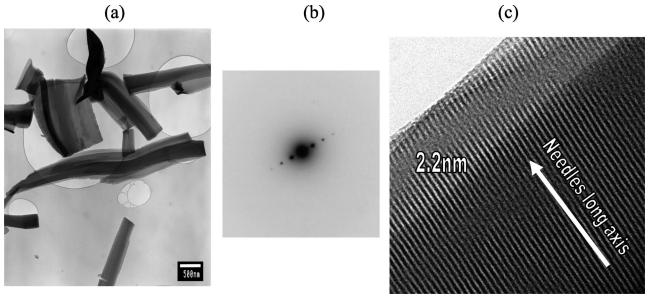

Figure 5. (a) TEM image of compound **A** (magnification: 12 000), at 80 kV. The inset bar corresponds to 500 nm. (b) SAED pattern of the central needle, at 80 kV with a camera length of 50 cm. (c) High-resolution TEM image (magnification: 200 000) of a needle obtained at 200 kV, showing a periodic spacing close to 22 Å.

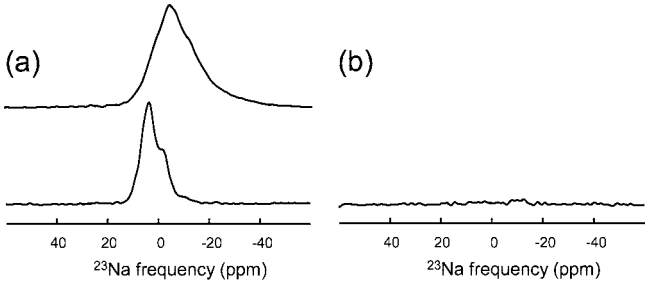

Figure 6. (a) ^{23}Na MAS NMR spectra of **TCP**+**A** recorded at 9.4 (top) and 17.6 T (bottom) with a spinning frequency of 12 kHz. (b) ^{23}Na MAS NMR spectra of **TCP**+**B** recorded at 17.6 T (12 kHz spinning frequency).

^{23}Na NMR resonances with second-order quadrupolar line shapes. However, the number of crystallographically nonequivalent sodium sites in the structure of compound **A** could not be unambiguously determined from the simulation of these MAS NMR spectra. Attempts to investigate the number of sodium sites using a MQMAS NMR experiment[53] were unsuccessful due to a fast dephasing of ^{23}Na NMR coherences, leading to a rather inefficient excitation of triple-quantum coherences and a broadening in the indirect dimension of the MQMAS NMR spectrum. It should also be mentioned that the weak signal in the ∼−10 ppm range in the ^{23}Na MAS NMR spectra recorded at 17.6 T accounts for the presence of low sodium contamination of the starting β-TCP.[54]

The protonation state of the four nonequivalent Zoledronate molecules in the unit cell of compound **A** was also studied using ^{31}P−^{1}H heteronuclear correlation (HETCOR)[45] NMR experiments, with FSLG decoupling to obtain high-resolution solid-state ^{1}H NMR spectra.[48,55] In addition to proton signals in the ∼4–9 ppm range related to the carbon backbone of Zoledronate, the 2D ^{1}H FSLG NMR spectrum of **TCP**+**A** (experimental data available in the Supporting Information) showed two narrow resonances at 1.2 and 3.4

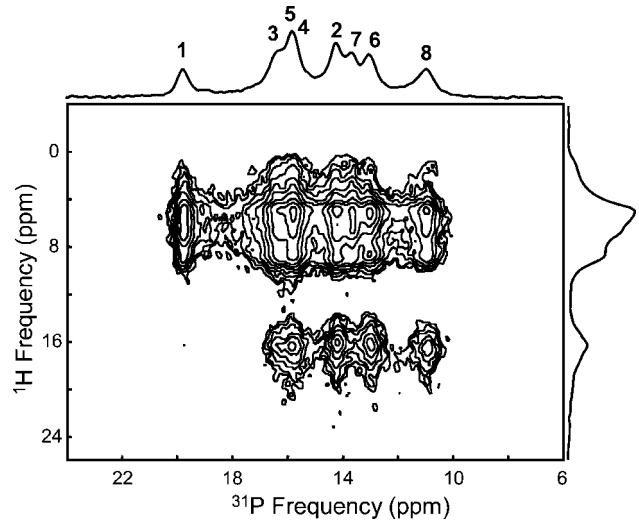

Figure 7. ^{31}P−^{1}H CP-LG HETCOR MAS NMR spectrum with FSLG decoupling of **TCP**+**A** recorded using a contact time of 750 μs at a magnetic field of 17.6T and a spinning frequency of 12 kHz.

ppm related to water molecules[56] and a broader resonance at 16.2 ppm assigned to P−OH sites. This assignment was supported by the ^{31}P−^{1}H {FSLG} and ^{13}C−^{1}H {FSLG} HETCOR MAS NMR spectra of the starting Zoledronate (see the Supporting Information), which showed ^{1}H NMR resonances at 15.4 and 18.2 ppm for the P−OH protons, ∼3.8 ppm for COH, 4.5 ppm for CH_2, and 7.6 ppm for the $C_3N_2H_3$ ring. It should be noted that the ^{1}H NMR isotropic chemical shifts of the P−OH resonances in compound **A** (16.2 ppm) and the starting Zoledronate (15.4 and 18.2 ppm) are significantly higher than those reported for P−OH sites in $CaHPO_4$ (13 and 15 ppm),[57] thus indicating the presence of strong hydrogen bonding.[58]

The location of the phosphonic acid protons in **A** was then investigated, using ^{31}P−^{1}H {FSLG} HETCOR MAS NMR spectra with Lee−Goldburg CP (CP-LG), in order to suppress ^{1}H NMR spin diffusion during the polarization transfer[46,47] (Figure 7). While all of the phosphorus sites [P(1)−P(8)] showed correlation with the ^{1}H NMR resonances of the carbon backbone, no correlation lines were observed between the phosphonic acid protons and the P(1), P(4), and P(7) sites, which could be assigned to deprotonated phosphonate groups. Moreover, the intensities of the cross-correlation peaks were similar for P(2), P(5), P(6), and P(8) sites (Table 2) but somewhat lower for P(3), thus indicating a longer H−P distance, consistent with hydrogen bonding [′P−O−H···O−P(3)′]. Accordingly, these results suggest that half of the eight phosphonate sites in compound **A** would be protonated, in agreement with the $CaNa[(HO)(C_4H_5N_2)C(PO_3)(PO_3H)]\cdot xH_2O$ proposed formulation, and that the corresponding four nonequivalent Zoledronate molecules present in the unit cell would have different protonation states and environments.

Behavior of TCP+A **in an Aqueous Medium.** In order to investigate the potential of **TCP**+**A** as a drug delivery

(53) Frydman, L.; Harwood, J. S. *J. Am. Chem. Soc.* **1995**, *117*, 5367–5368.
(54) Obadia, L.; Deniard, P.; Alonso, B.; Rouillon, T.; Jobic, S.; Guicheux, J.; Julien, M.; Massiot, D.; Bujoli, B.; Bouler, J.-M. Effect of sodium doping in b-Tricalcium phosphate on its structure and properties. *Chem. Mater.* **2006**, *18*, 1425–1433.
(55) van Rossum, B. J.; Förster, H.; de Groot, H. J. M. *J. Magn. Reson., Ser. A* **1997**, *124*, 516.
(56) Alam, T.; Tischendorf, B. C.; Brow, R. K. *Solid State NMR* **2005**, *27*, 99–111.
(57) Jäger, C.; Welzel, T.; Meyer-Zaika, W.; Epple, M. *Magn. Reson. Chem.* **2006**, *44*, 573–580.
(58) Brunner, E.; Sternberg, U. *Prog. Solid State NMR* **1998**, *32*, 21–57.

Table 2. Relative Intensities of the Cross-Correlation Peaks between the Two ^{31}P NMR Resonances and the One ^{1}H NMR Resonance of the P−OH Groups [*I*(P−OH)] and of the Carbon Backbone [*I*(P backbone)] for the Nonequivalent Zoledronate Molecules in Compounds A and B, Determined from the ^{31}P−^{1}H {FSLG} CP-LG HETCOR MAS NMR Spectra of TCP+A and TCP+B(Figures 6 and 7)

sample	Zoledronate molecule	P site	δ_{ISO} (ppm)	*I*(P−OH)	*I*(P backbone)
TCP+A	I	P(1)	19.7	0.05	0.95
		P(2)	14.2	0.30	0.70
	II	P(3)	16.4	0.20	0.80
		P(4)	15.5	0.05	0.95
	III	P(5)	15.8	0.30	0.70
		P(6)	12.9	0.30	0.70
	IV	P(7)	13.6	0.05	0.95
		P(8)	10.9	0.35	0.65
TCP+B	I	P(1)	15.6	0.25	0.75
		P(2)	14.6	0.10	0.90

system, its solubility was studied, assuming that the BP release should mirror the solubility constant of compound **A**. When **TCP+A** was suspended in water (500 mg in 10 mL) for 1 h, the amount of Zoledronate measured in the liquid phase was high (ca. 25% of Zoledronate initially present on the solid), thus suggesting that **TCP+A** is of low practical interest for its use as a tool for the controlled release of the BP. Surprisingly, successive equilibrations of this material in a renewed aqueous solution showed that the amount of BP released decreased after each cycle, to drop under the detection limit of the TOC analyzer ($C_{Zoledronate} < 8 \times 10^{-6}$ mol L^{-1}) after cycle no. 5, while a significant amount of residual Zoledronate was still present on the solid [56.7(6)%].

Therefore, the resulting solid (termed as **TCP+B**) was isolated at this stage and a ^{31}P CP MAS NMR spectrum was recorded, giving evidence of a transformation of complex **A** into a new complex (termed as **B**) because only two nonequivalent phosphorus sites were observed, along with a significant broadening of the ^{31}P NMR resonances (Figure 3c and Table 1). The indexation of the powder XRD pattern recorded for **TCP+B** showed the presence of crystalline β-TCP as the major product, with only one additional weak diffraction peak observed at high θ values (12.3 Å), most likely corresponding to compound **B**. The TGA curve of **TCP+B** consisted of a first endothermic step (78 °C) most likely corresponding to the release of water molecules (observed weight loss: 2.0%). Then, a complicated stepwise process of hydrogen phosphonate group condensation and burning of organic moieties occurs between 100 and 800 °C (three DSC exothermic peaks observed at 320, 465, and 660 °C, respectively). The transformation is completed at 800 °C, resulting in a white solid after a total weight loss of 6.6%. Identification of the decomposition product of complex **B** was not possible from the powder XRD pattern of the residue, which was dominated by the β-TCP diffraction peaks.

Complex **B** was found to be a single phase, using 2D ^{31}P NMR homonuclear through-space DQ−SQ correlation experiments (data not shown). However, SEM observations did not show any change in the morphology of the sample, and it was possible again to separate a small amount of material by sonication in ethanol, which consisted mainly of the

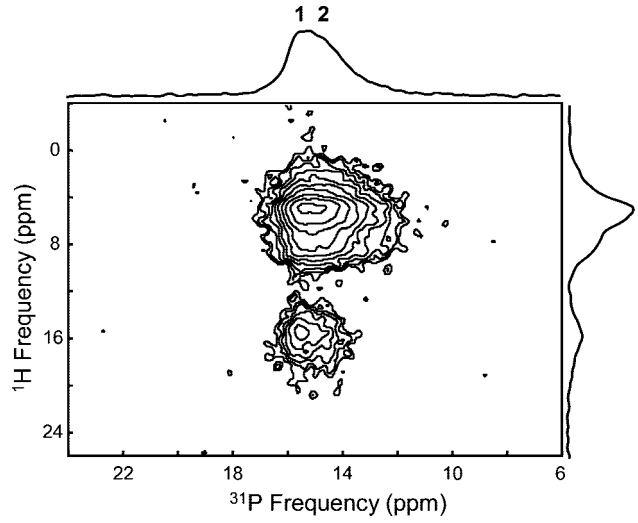

Figure 8. ^{31}P−^{1}H CP-LG HETCOR MAS NMR spectrum with FSLG decoupling of **TCP+B**, recorded using a contact time of 750 μs at a magnetic field of 17.6 T and a spinning frequency of 12 kHz.

crystalline phase. EDXS analyses of the crystalline needles of compound **B** led to a P/Ca/Na ratio [2:1.45(10):0.14(8)] that gave evidence of a pure Zoledronate calcium complex, with the probable following composition: $Ca_3[(HO)(C_4H_5N_2)C(PO_3)(PO_3H)]_2 \cdot xH_2O$. Among calcium aminobisphosphonate complexes reported in the literature, such as Ca(ABP), $Ca(ABP)_2$, and $Ca_4(ABP)_3$ (ABP = alendronate),[59–61] none with a stoichiometry similar to that found in compound **B** was described. The absence of sodium in this complex was confirmed by recording the single-pulse ^{23}Na MAS NMR spectrum of **TCP+B** (Figure 6b), which showed only the very weak resonance related to the low sodium contamination present in the starting β-TCP phase. Moreover, the ^{31}P−^{1}H {FSLG} CP-LG HETCOR MAS NMR spectrum of **TCP+B** (Figure 8) suggested that the phosphonic acid proton (δ_{ISO} = 15.1 ppm) is likely present on only one of the two phosphorus sites [P(1); see Table 2]. However, because of the broadening of the two ^{31}P NMR resonances, a distribution of the protons on the two phosphorus sites cannot be totally excluded.

In Vitro Biological Evaluation of TCP+B. The evaluation of the biological activity of Zoledronate-loaded materials required the development of an in vitro bone resorption model. Various osteoclastic models have been previously described.[62] Among these models, previous reports indicate that the unfractioned rabbit bone cell model is one of the most convenient.[37,38,63,64] This bone resorption assay sup-

(59) Brenner, G. S.; Ostovic, D. Use of bisphosphonic acids for the treatment of calcium metabolism disorders. EP 0449405, 1991.
(60) Fernandez, D.; Vega, D.; Goeta, A. Alendronate zwitterions bind to calcium cations arranged in columns. *Acta Crystallogr., Sect. C: Cryst. Struct. Commun.* **2003**, *59*, M543–M545.
(61) Matczak-Jon, E.; Videnova-Adrabinska, V. Supramolecular chemistry and complexation abilities of diphosphonic acids. *Coord. Chem. Rev.* **2005**, *249* (21–22), 2458–2488.
(62) Heymann, D.; Guicheux, J.; Gouin, F.; Passuti, N.; Daculsi, G. Cytokines, growth factors and osteoclasts. *Cytokine* **1998**, *10* (3), 155–168.
(63) David, J. P.; Neff, L.; Chen, Y.; Rincon, M.; Horne, W. C.; Baron, R. A new method to isolate large numbers of rabbit osteoclasts and osteoclast-like cells: Application to the characterization of serum response element binding proteins during osteoclast differentiation. *J. Bone Miner. Res.* **1998**, *13* (11), 1730–1738.

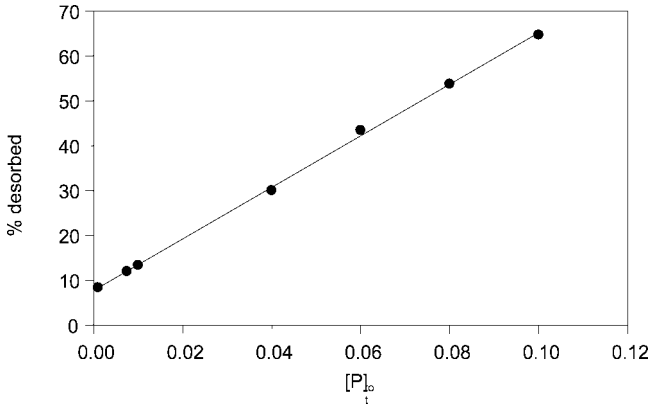

Figure 9. Desorption study on **TCP+B** in phosphate buffers: percentage of Zoledronate released as a function of the phosphate concentration of the buffer, S/L = 2 g L^{-1}.

ports the formation and activity of mature resorbing osteoclasts,[37] which is characterized by pit formation on dentin slices.

Assuming that **TCP+A** would release Zoledronate at a cytotoxic level, the evaluation of the biological activity of the Zoledronate-loaded materials was focused on **TCP+B**. Indeed, for the latter phase, the BP release in water was found to be very low (under the detection limit of the TOC analyzer), while interestingly the release was directly related to the phosphate concentration when performed in phosphate buffers (Figure 9; e.g., $\sim 3 \times 10^{-5}$ mol L^{-1} for S/L = 2 g L^{-1} in a 10^{-3} mol L^{-1} phosphate buffer). The XRD pattern and ^{31}P CP MAS NMR spectrum recorded for a sample of **TCP+B** desorbed in a 4×10^{-2} mol L^{-1} phosphate buffer were similar to those of **TCP+B** before desorption, with a weakening of the features related to complex **B**. This observation suggests that a dissolution of compound **B** takes place, driven by the displacement of the BP by phosphate ions.

To determine whether **TCP+B** might be effective in inhibiting osteoclastic resorption, the effect of **TCP+B** [diluted in pure TCP (1:1000)] on the osteoclastic resorption activity on dentin slices was investigated and compared with the most effective in vitro concentration of Zoledronate (10^{-6} mol L^{-1}). It is worth noting that for 1:1000 diluted **TCP+B**, a full release of the BP in the culture medium would result in a 1.4×10^{-5} mol L^{-1} Zoledronate concentration in the solution.

In our untreated osteoclast-like cell culture, we observed a high resorption activity on the surface of dentin slices as evidenced by the high number of large resorption lacunae formed (data not shown). In comparison, our results showed that 1:1000 diluted **TCP+B** is as effective as 10^{-6} mol L^{-1} Zoledronate (six-fold decrease in the resorbed dentin surface), suggesting that only a fraction of the Zoledronate loaded is released (ca. 7%). Both exhibit an almost complete and very similar and significant inhibition of osteoclastic resorption ($p < 0.05$; Figure 10). It is thus reasonable to assume that such materials could provide a drug release at low concentration over a long period, and to confirm this, their in vivo evaluation is currently in progress, using animal osteoporosis models (rats, ewes, etc.).

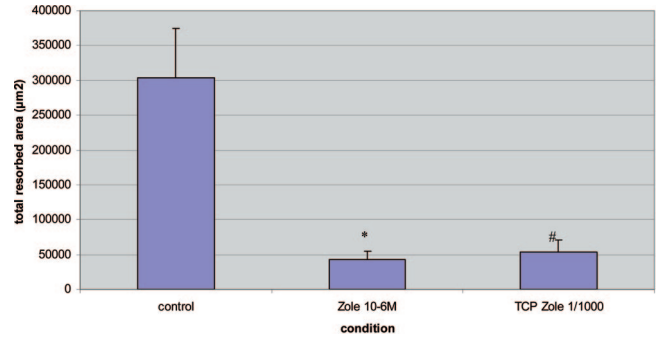

Figure 10. Evaluation of the biological activity of **TCP+B**. A total rabbit bone cell preparation was established on dentin slices (see the Experimental Section). Cell preparation was then cultured for 4 days in the presence of 1:1000 diluted **TCP+B** pellets. A fresh 10^{-6} mol L^{-1} Zoledronate solution was used as the internal reference. Control corresponded to cells exposed to the culture medium. Dentin slices were next prepared for SEM observation linked to a semiautomatic image analyzer. Resorption activity of osteoclasts is expressed as the total surface resorbed of the dentin slice. Results are the mean ± SEM of six independent experiments. *,#: $p < 0.05$ as compared to the control.

Conclusion

Bone implants are widely used in orthopedics and dentistry to treat hard tissue disorders. Surface modifications of those implants are under intense investigation for various applications, including the local delivery of pharmaceuticals.[65] In this context, our recent research has been focused on the design of *gem*-BP delivery systems applicable to osteoporosis therapy and based on the chemical association of the drug with calcium phosphate bone reconstruction implants used as the carrier phase. Indeed, BPs are potent antibone resorption agents and are currently the preferred choice in clinics for treating osteoporotic patients in order to prevent osteoporosis-related bone fracture. In the present paper, we have studied the reaction of one type of *gem*-BP (Zoledronate) with β-TCP using various experimental techniques, including modern high-resolution solid-state NMR, which is a powerful tool for probing the chemical environment of the BP moiety in BP/calcium phosphate composites. We have shown that this reaction led to the precipitation of a crystalline mixed calcium and sodium complex, resulting from a partial dissolution of β-TCP. This complex was found to be a metastable phase that transformed into a calcium bisphophonate complex upon repeated washings with water. While this latter composite material was poorly soluble in water, the release of low doses of BP was observed in phosphate media in direct proportion to the phosphate concentration. This suggests that when **TCP+B** is implanted in bone tissues, the BP will be released in greater concentration, the more the bone is being resorbed (resulting in a large release of phosphate into the extracellular matrix), i.e., just when the drug is needed to decrease osteoclast activity. Moreover, our preliminary in vitro results suggest that this

(64) Tezuka, K.; Sato, T.; Kamioka, H.; Nijweide, P. J.; Tanaka, K.; Matsuo, T.; Ohta, M.; Kurihara, N.; Hakeda, Y.; Kumegawa, M. Identification Of Osteopontin In Isolated Rabbit Osteoclasts. *Biochem. Biophys. Res. Commun.* **1992**, *186* (2), 911–917.

(65) Duan, K.; Wang, R. Z. Surface modifications of bone implants through wet chemistry. *J. Mater. Chem.* **2006**, *16* (24), 2309–2321.

type of BP-modified β-TCP might be suitable for practical application as a BP local delivery system and might overcome the associated side effects sometimes observed in osteoporotic patients receiving BP intravenous administration.

Acknowledgment. This work was partially supported by the French Ministry of Research (ACI "Technologies pour la Santé"), the CNRS (Programme "Matériaux Nouveaux—Fonctionnalités Nouvelles"), and ANR (RNTS programme, Contract 5A 0659). Partial support from the Région Pays de la Loire (CER "Biomatériaux S3") is also acknowledged. We thank Novartis Pharma Research (Basel, Switzerland) for a generous gift of Zoledronate and J. R. Green (Novartis Pharma Research) for fruitful discussion. The authors thank the "Institut des Matériaux Jean Rouxel" (UMR CNRS 6502) for access to TEM facilities (Hitachi HF2000), and Dr. F. Christien from the "Laboratoire de Génie des Matériaux et de Procédés Associés" (Ecole Polytechnique de l'Université de Nantes) for his helpful contribution to EPMA. Dr. G. Montavon (UMR CNRS 6457, Subatech) is greatly acknowledged for the TOC measurements.

Supporting Information Available: 2D ^{1}H FSLG MAS NMR spectra of the starting Zoledronate, **TCP**+**A** and **TCP**+**B** (Figure SI); 2D ^{31}P−^{1}H {FSLG} CP-LG and 2D ^{13}C−^{1}H {FSLG} VACP HETCOR MAS NMR spectra of the starting Zoledronate (Figure SII); EPMA spectra obtained with the WDS for **TCP**+**A** and Zoledronate powders (Figure SIII); powder XRD pattern of **TCP**+**B** (Figure SIV); TGA/DSC curves of **TCP**+**A** (Figure SV) and **TCP**+**B** (Figure SVI); ^{31}P CP MAS NMR spectra recorded for a sample of **TCP**+**B** before and after desorption in a 4×10^{-2} mol L^{-1} phosphate buffer (Figure SVII). This material is available free of charge via the Internet at http://pubs.acs.org.

CM702584D